PHILOSOPHICAL TRANSACTIONS OF THE ROYAL SOCIETY A MATHEMATICAL, PHYSICAL & ENGINEERING SCIENCES

Influence of stochastic sea ice parametrization on climate and the role of atmosphere–sea ice–ocean interaction

Stephan Juricke and Thomas Jung

Phil. Trans. R. Soc. A 2014 **372**, 20130283, published 19 May 2014

PHILOSOPHICAL TRANSACTIONS OF THE ROYAL SOCIETY A

rsta.royalsocietypublishing.org

Research

Cite this article: Juricke S, Jung T. 2014 Influence of stochastic sea ice parametrization on climate and the role of atmosphere–sea ice–ocean interaction. *Phil. Trans. R. Soc. A* **372**: 20130283.
http://dx.doi.org/10.1098/rsta.2013.0283

One contribution of 14 to a Theme Issue 'Stochastic modelling and energy-efficient computing for weather and climate prediction'.

Subject Areas:
oceanography

Keywords:
stochastic parametrizations, sea ice models, sea ice strength, model uncertainty, atmospheric feedbacks

Author for correspondence:
Stephan Juricke
e-mail: stephan.juricke@awi.de

Royal Society Publishing

Influence of stochastic sea ice parametrization on climate and the role of atmosphere–sea ice–ocean interaction

Stephan Juricke and Thomas Jung

Alfred Wegener Institute, Helmholtz Centre for Polar and Marine Research, Bremerhaven, Germany

The influence of a stochastic sea ice strength parametrization on the mean climate is investigated in a coupled atmosphere–sea ice–ocean model. The results are compared with an uncoupled simulation with a prescribed atmosphere. It is found that the stochastic sea ice parametrization causes an effective weakening of the sea ice. In the uncoupled model this leads to an Arctic sea ice volume increase of about 10–20% after an accumulation period of approximately 20–30 years. In the coupled model, no such increase is found. Rather, the stochastic perturbations lead to a spatial redistribution of the Arctic sea ice thickness field. A mechanism involving a slightly negative atmospheric feedback is proposed that can explain the different responses in the coupled and uncoupled system. Changes in integrated Antarctic sea ice quantities caused by the stochastic parametrization are generally small, as memory is lost during the melting season because of an almost complete loss of sea ice. However, stochastic sea ice perturbations affect regional sea ice characteristics in the Southern Hemisphere, both in the uncoupled and coupled model. Remote impacts of the stochastic sea ice parametrization on the mean climate of non-polar regions were found to be small.

1. Introduction

Accurately simulating sea ice is an essential part of coupled Earth system modelling. Sea ice has a strong impact on the heat and momentum exchange between

the atmosphere and ocean. As an insulating layer, sea ice can partially decouple the atmosphere from the ocean, and through the albedo feedback, it influences the radiation balance at the surface.

Sea ice also alters the freshwater content of the upper ocean and hence ocean deep convection; therefore, sea ice is an important driver of changes in the global overturning circulation of the ocean. Sea ice is also considered to be a main factor for the Arctic amplification of anthropogenic climate change.

Sea ice is known to show changes on a wide range of temporal scales. There is evidence, for example, for high interannual variability, both locally [1] and Arctic wide [2]. Furthermore, recent years have shown a strong decrease in Arctic sea ice volume [3,4] and area, which is only partly captured by models [5–7]. Potential predictability studies for the Arctic reveal the importance of an accurate simulation of the prevailing sea ice thickness conditions to allow for skilful seasonal and interannual predictions of Arctic sea ice [8,9].

To simulate sea ice thickness and concentration fields realistically, it is crucial to adequately capture the drift of the sea ice [10]. Sea ice drift is strongly influenced by the sea ice dynamics which, in turn, hinges on the formulation of the sea ice rheology that describes the deformation behaviour in the presence of convergent flow. Most climate models use the widely used viscous-plastic rheology by Hibler [11] or the modified elastic-viscous-plastic rheology [12]; other formulations are being tested [13], and different ways of solving the highly nonlinear equations are emerging from the viscous-plastic formulation [14,15]. Still, all existing parametrizations have certain shortcomings when it comes to the representation of sea ice deformation and the resulting sea ice drift. Therefore, the sea ice rheology has to be considered as a significant source of uncertainty in coupled climate models.

In the past two decades or so, the representation of model uncertainty in models has become a major area of research. Studies with simplified models such as the Lorenz '96 system [16] emphasize the importance of developing and analysing stochastic parametrizations as a promising alternative to determinstic schemes [17,18]. A lot of progress in this field has been made in atmospheric modelling and especially weather forecasting. Different studies have shown the importance of stochastic approaches when it comes to accounting for model uncertainty and for accurately representing subgrid scale processes. Approaches range from estimating the accumulated physical tendency uncertainty in the formulations of the discretized prognostic equations [19,20] to a stochastic kinetic energy backscatter scheme which simulates the backscatter of dissipated energy from unresolved to resolved scales [21–23]. Moreover, stochastic parametrizations have been developed for non-orographic gravity waves [24], convection [25] and deep convection [26]. In addition, stochastic perturbations have been applied to a variety of parameters within determinstic parametrizations [27–29].

While the emphasis of previous research has been on the atmosphere, more recently stochastic approaches have also been developed for other parts of the Earth system. Examples include the stochastic representation of the ice strength parameter in sea ice–ocean models [30], the use of stochastic perturbations for oceanic temperature and salinity fields in the computation of the horizontal density field [31] and the stochastic representation of turbulent surface fluxes at the atmosphere–ocean interface in a coupled model [32]. Those studies demonstrate that the explicit representation of model uncertainty in models has not only the benefit of improved ensemble prediction capabilities, but that stochastic parametrizations also have the potential to change the climate of models. It has been argued, therefore, that stochastic parametrizations should be incorporated in the next generation of climate models [33].

In this study, the influence of using stochastic dynamical formulations in sea ice models will be further explored building on the work of Juricke *et al.* [30], in which stochastic perturbations have been applied to the sea ice strength parametrization of the sea ice rheology formulation in a sea ice–ocean model. Here, a slightly modified stochastic parametrization is tested. Furthermore, it is investigated whether the substantial changes in the mean climate state caused by the stochastic sea ice parametrizations in a sea ice–ocean model found by Juricke *et al.* [30] also translate to fully coupled climate models. It is of importance, also for future ensemble simulations, to be aware of any impact on the mean climate owing to uncertainty estimates in parametrizations

and in this context to understand effects of perturbations in highly nonlinear systems. This study also aims at detecting the possibly differing impacts in the more complex coupled system compared with uncoupled models. To this end, the coupled atmosphere–ocean–sea ice–land surface system ECHAM6-FESOM is used in a configuration with relatively high resolution in the Arctic ocean [34]. More specifically, single climate simulations are conducted to analyse the impact of the stochastic parametrization on the mean state of the system. The atmospheric fluxes generated by a coupled reference simulation are then used to carry out experiments with the uncoupled sea ice–ocean model with stochastic sea ice strength parametrization. In this way, it is possible to explore the role of atmospheric feedback processes in determining the response of the climate system to stochastic sea ice perturbations. As only one single parametrization is affected by perturbations, it is still feasible to find some detailed physical explanations for the workings and effects of the perturbations on sea ice variables in the uncoupled as well as the coupled system.

The structure of this paper is as follows: §2 gives a short summary of the model and the stochastic parametrization, including a description of the modification of the spatial correlation procedure for the stochastic perturbations originally developed by Juricke *et al.* [30]. Furthermore, the experimental set-up is explained. In §3, the impact of the stochastic parametrization on the global mean climate is analysed and discussed. Detailed explanations of the differing effects in the coupled and uncoupled simulations are given. Finally, §4 gives a summary, some concluding remarks and an outlook for future work.

2. Experimental set-up

In this study, the coupled model ECHAM6-FESOM is used. ECHAM6 is the spectral atmospheric climate model of the Max Planck Institute for Metereology in Hamburg [35]. It is coupled through the OASIS3-MCT coupler [36] to the finite-element sea ice ocean model (FESOM) of the Alfred Wegener Institute in Bremerhaven [37–41]. While ECHAM6 uses a T63L47 grid with a resolution of about 1.85° and 47 vertical levels, FESOM uses an unstructured triangular finite-element grid for the ocean surface and the sea ice model, with resolutions ranging from over 150 km in the open oceans to about 25–10 km in the Arctic and near the coasts. In addition, there is a gradual increase in resolution along the equatorial belt in the tropics to about 25 km (see fig. 1 in [34]). The three-dimensional ocean model uses a tetrahedral grid of 46 unevenly spaced z-levels. The timestep of FESOM is 30 min, whereas ECHAM6 uses a timestep of 10 min. Coupling takes place every 6 h. Further details on ECHAM6-FESOM, its set-up and mean-state performance are discussed by Sidorenko *et al.* [34]. The climate variability of the model is described in Rackow *et al.* [42].

The prognostic variables of the sea ice model are the effective (mean) sea ice thickness, h_{ice}, the lateral sea ice velocities, u_{ice} and v_{ice}, and the sea ice concentration, A, as well as the mean snow layer thickness, h_{s}. The evolution of h_{ice}, h_{s} and A is described by equations for advection as well as freezing and melting processes. Changes in sea ice velocities are calculated using the equation of momentum balance.

(a) Stochastic sea ice strength parametrization

The stochastic parametrization used in this study is described in detail by Juricke *et al.* [30]. In the following, therefore, only a brief explanation is given, and differences to the original formulation are highlighted.

The equation of momentum balance for the lateral sea ice velocities is given by

$$m\frac{\partial \boldsymbol{u}_i}{\partial t} = \boldsymbol{\tau}_{\mathrm{air}} + \boldsymbol{\tau}_{\mathrm{ocean}} - mf\boldsymbol{k}\times\boldsymbol{u}_i - mg\nabla\eta_{\mathrm{o}} + \boldsymbol{F}_{\mathrm{int}}. \tag{2.1}$$

In (2.1), m is the mass per unit area, $\boldsymbol{u}_i$ is the horizontal sea ice velocity vector, $\boldsymbol{\tau}_{\mathrm{air}}$ and $\boldsymbol{\tau}_{\mathrm{ocean}}$ are the atmospheric and oceanic stress, respectively, f is the Coriolis parameter, $\boldsymbol{k} = (0, 0, 1)$, g is the gravitational acceleration and η_{o} is the sea surface height of the ocean.

The internal forces $\boldsymbol{F}_{\text{int}} = (F_1, F_2)$ are parametrized using the highly nonlinear elastic–viscous–plastic rheology [12] which is based on the viscous–plastic rheology by Hibler [11]. Some further adjustments have been made by Harder [43]. Within this parametrization, the so-called internal ice strength P can be interpreted as a regularization factor for the yield curve which describes all possible combinations of stresses that lead to the yielding of the sea ice. Therefore, large values of P lead to an increased resistance of the ice when it comes to convergent motion, whereas small values of P produce weaker sea ice and an earlier onset of plastic deformation. This, by changes in the sea ice velocities, leads to a piling up of sea ice and an increase of sea ice thickness. P itself depends linearly on the factor P_p given by

$$P_p = P^* \frac{h_{\text{ice}}}{A} \cdot \exp(-C(1-A)), \tag{2.2}$$

where P^* and C are dynamic ice strength parameters.

To account for uncertainties in the choice of the empirical parameter P^*, including temporal and spatial variability, Juricke *et al.* [30] have applied a symmetric Markov process time and space correlated perturbation (MTSP) to P^*. Adjustments to the spatial correlation of the perturbations are outlined in the following.

For each timestep j and node i of the ice covered triangular surface mesh, a new value,

$$P^*(i,j) = (1 + x(i,j)) \cdot P^*_{\text{ref}}, \tag{2.3}$$

is calculated. $P^*_{\text{ref}} = 30\,000\,\text{N}\,\text{m}^{-2}$ is the reference value of the regular deterministic parametrization and $x(i,j)$ is a random number from a symmetric distribution with zero mean. In addition, $x(i,j) \in (-0.75, 0.75)$ and therefore $P^*(i,j) \in (7500\,\text{N}\,\text{m}^{-2}, 52\,500\,\text{N}\,\text{m}^{-2})$. Note that the value for P^*_{ref} in the three simulations of this study differs from the value of $20\,000\,\text{N}\,\text{m}^{-2}$ used in MTSP by Juricke *et al.* [30]. As P^* is one of the tuning parameters of the sea ice model, it was used to adjust sea ice extent and volume in the coupled set-up.

In summary, equation (2.3) describes a random perturbation of a previously fixed parameter. To create spatially and temporally correlated perturbations $x(i,j)$ with a bounded distribution, transformations of Gaussian random numbers are used. First, time correlation is generated by

$$y(i,j) = \alpha y(i,j-1) + z(i,j), \tag{2.4}$$

with autocorrelation $\alpha = 0.994$ and $z(i,j)$ an uncorrelated Gaussian-distributed random number with zero mean and standard deviation $\sigma = 0.375$. The timestep of the ocean and sea ice model is $\Delta t = 30\,\text{min}$. These values are within the range of values tested in Juricke *et al.* [30] even though they differ slightly from their preferred parameter choice, implying a slightly larger maximum variance σ^2_{lim} (for $j \to \infty$) for the autoregressive process in (2.4).

The values $y(i,j)$ are then spatially correlated using two correlation matrices C_{NH} and C_{SH}, one for the nodes above 45° and one for below −45°, respectively, to ensure that the Northern Hemisphere (NH) and Southern Hemisphere (SH) sea ice are uncorrelated. The entries of each matrix are given by $C^{nm}_X = \text{e}^{-d_{nm}/d_{\text{corr}}}$, $X = \{NH, SH\}$, where d_{nm} is the distance between node n and m, from the respective hemisphere, and $d_{\text{corr}} = 1000\,\text{km}$ for both matrices. For this new spatial correlation scheme, $d_{\text{corr}} = 1000\,\text{km}$ was chosen to produce large-scale patterns in the variations of P^* and possibly maximize the impact of the perturbations.

Using the Cholesky decompositions of C_{NH} and C_{SH}, spatially correlated $\hat{y}(i,j)$ can now be generated for both hemispheres from the temporally correlated $y(i,j)$, by simple matrix–vector multiplication. As the resulting random numbers are still Gaussian distributed, the transformation

$$x(i,j) = -a + \frac{2a}{1 + \text{e}^{(-\beta \hat{y}(i,j))}} \tag{2.5}$$

transforms the numbers into the limited range $(-a, a)$ with $a = 0.75$ and $\beta = 1/\sigma_{\text{lim}}$ with $\sigma_{\text{lim}} = \sqrt{\sigma^2/(1-\alpha^2)}$ [30]. For the initialization of the random numbers, equation (2.4) is solved successively a couple of thousand times at the beginning of each climate simulation to reach this maximum standard deviation of the autoregressive process.

Table 1. Summary of the experiments used in this study.

name	stochastic	coupled	years
REF	no	yes	201
STOCH_UNCPL	yes	no	102
STOCH_CPL	yes	yes	201

(b) Simulations

To investigate the impact of the stochastic parametrization several multi-decadal integrations have been carried out. A simulation with the coupled ECHAM6-FESOM model *without* stochastic sea ice parametrization serves as the reference integration (REF hereafter). The surface flux fields from REF, saved for every 6 hourly coupling timestep, were used to drive FESOM in uncoupled mode with the stochastic sea ice parametrization switched on (STOCH_UNCPL hereafter). This integration allows for a direct evaluation of the impact of stochastic sea ice parametrization on sea ice distribution and ocean currents without an interactive atmosphere. To analyse the impact of atmospheric feedbacks another experiment with the coupled model ECHAM6-FESOM has been carried out in which the stochastic sea ice strength parametrization has been switched on (STOCH_CPL). The uncoupled experiment STOCH_UNCPL was run for a period of 102 years; the two coupled integrations were extended to 201 years in order to account for the larger uncertainty generated by having two completely different realizations of the atmospheric trajectory (table 1). Note that all parameter values and parametrizations in FESOM for STOCH_UNCPL and STOCH_CPL are exactly the same, except for the sequences of random numbers that are used. In addition, initial conditions for all three simulations are the same.

3. Results

In the following, the impact of the stochastic sea ice strength perturbations are described separately for Arctic and Antarctic sea ice. Effects on integrated quantities such as sea ice volume as well as regional impacts on variables such as sea ice thickness are analysed. Some explanations on how the stochastic sea ice strength perturbation affect Arctic and Antarctic sea ice will be proposed, focusing on the differing impacts of the stochastic parametrization in the uncoupled compared with the coupled simulation. Furthermore, the remote influence of the stochastic scheme on the climate in non-polar regions is explored.

(a) Arctic sea ice

(i) Volume

Figure 1, *a*(i,ii) shows the Northern Hemisphere sea ice volume and area of the two stochastic simulations and the reference simulation REF for March and September. Evidently, ECHAM6-FESOM simulates substantial Arctic sea ice variability throughout the year across a wide range of timescales. This appears to be rather consistent with observations and is discussed in more detail in Sidorenko *et al.* [34] and especially by Rackow *et al.* [42]. The Arctic sea ice volume in the uncoupled set-up STOCH_UNCPL is highly correlated to that of REF owing to the fact that the sea ice has experienced effectively the same atmospheric forcing. However, STOCH_UNCPL shows a clear increase in Arctic sea ice volume when compared to REF (figure 1, (i)). The first 20–30 years can be seen as a transient phase during which Arctic sea ice volume builds up slowly. It is worth pointing out that the year-to-year increase in the sea ice volume is rather small during the transient phase; the fact that the quasi-equilibrium response in the Arctic owing to the stochastic sea ice scheme amounts to 10–20% after the first three decades of the integration can be explained through accumulation.

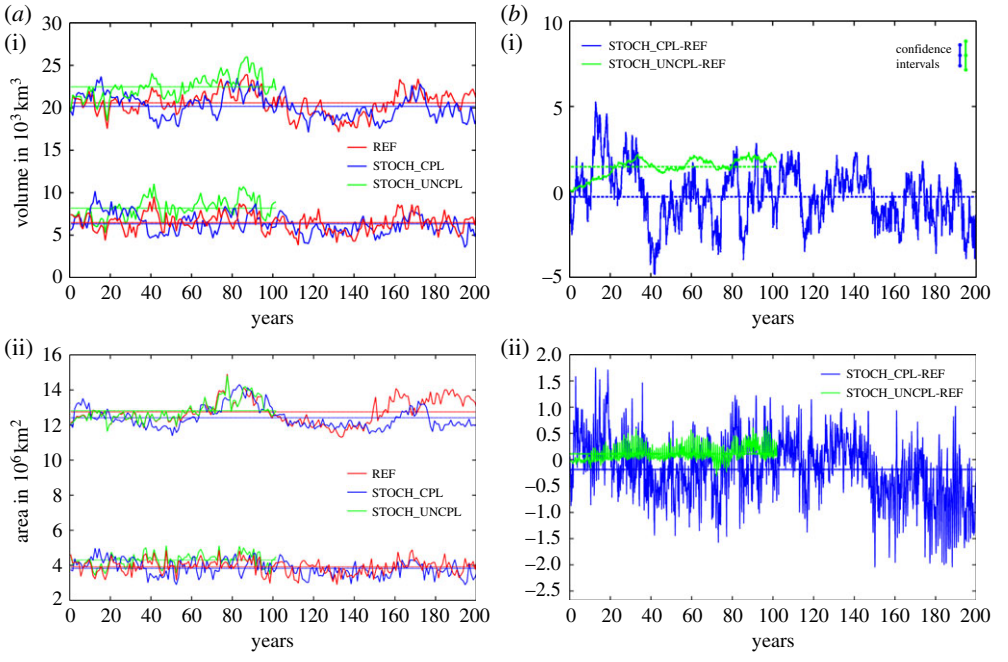

Figure 1. (*a*) Northern Hemisphere total (i) sea ice volume (10^3 km^3) and (ii) sea ice area (10^6 km^2) for REF (red), STOCH_CPL (blue) and STOCH_UNCPL (green); results are shown for March (upper curves) and September (lower curves). (*b*) Monthly mean difference in Northern Hemisphere (i) sea ice volume (10^3 km^3) and (ii) sea ice area (10^6 km^2) between STOCH_CPL and REF (blue) as well as STOCH_UNCPL and REF (green). Coloured horizontal lines show respective mean values. 95% confidence intervals—using a *t*-test with consideration of the reduction of effective sample size owing to a lag-1 autocorrelation [44]—are given as vertical bars.

A possible explanation for the increase in sea ice volume with the stochastic sea ice strength parametrization has been given by Juricke *et al.* [30]. In summary, the symmetric stochastic perturbations of the sea ice strength effectively lead to a weakening of the ice cover owing to the highly nonlinear formulation of the internal forces of the sea ice. Low P^* values are more effective at reducing sea ice strength and increasing plastic deformation under convergent drift than the high P^* values are at preventing sea ice from piling up. Newly created areas of open water owing to the increased drift then enable increased sea ice production. After the transient phase, during which the sea ice volume has increased, a new mean state is established in which increased sea ice volume counteracts the effective reduction of sea ice strength. The sea ice thickness distribution function of STOCH_UNCPL is shifted towards higher ice thicknesses (not shown). Because sea ice thickness as well as the P^* value act linearly on the value of the sea ice strength, larger ice thicknesses can compensate for low P^* values.

In contrast to the uncoupled experiment, the mean sea ice volume in STOCH_CPL shows a slight decrease compared with REF. The 95% CIs included in figure 1*b*(i) for the difference between STOCH_UNCPL and REF as well as STOCH_CPL and REF do not overlap. This indicates that the response of the Arctic sea ice volume to the stochastic sea ice parametrization in the coupled model is significantly different from that in the uncoupled set-up. This, in turn, suggests that a negative feedback involving the atmosphere is operating in the coupled system that prevents the Arctic sea ice volume from accumulating as observed in the uncoupled system. Given that the accumulation of sea ice in the uncoupled system is rather slow, a relatively weak negative atmospheric feedback would be sufficient to prevent the ice from accumulating in the coupled model. As a variety of strong feedback mechanisms are known to be present in the Arctic, it is difficult to provide a conclusive answer as to which negative feedback mechanism is crucial to

explain the above results. Nevertheless, at the end of this section, a possible negative feedback is proposed that could serve as an explanation for the above-mentioned results.

(ii) Area

Time series of Arctic sea ice area and changes therein owing to the use of the stochastic scheme are shown in figure 1*a*(ii),*b*(ii). STOCH_UNCPL shows a slight increase in area at the end of the transient phase whereas sea ice area does not show a discernable trend for STOCH_CPL. The strong seasonal dependence of the impact of the stochastic perturbations on sea ice area has been described in Juricke *et al.* [30] although the sign of the changes is different in this study. Juricke *et al.* [30] explained the sea ice area decrease by an increased drift, away from areas of low concentration and divergence, towards coastlines and generally the western Arctic. This leads to reduced sea ice concentrations along the ice edge and in the eastern Arctic. Basically, this explanation also holds for STOCH_UNCPL during the first few years, when the stochastic sea ice parametrization also reduced the sea ice area. It should be noted, though, that the length of the integration in Juricke *et al.* [30] is considerably shorter (17 years) and was forced by common ocean ice reference experiments (CORE) version 2 atmospheric forcing [45] which accounts for changes in atmospheric conditions owing to rising CO_2 concentrations.

(iii) Regional impacts

Figure 2 highlights the regional changes in Arctic sea ice thickness and concentration. The left column shows the annual mean sea ice thickness and concentration distribution of the Arctic for REF, years 1–201. The middle and right columns illustrate the differences in the two distributions between STOCH_UNCPL and REF for years 1–102 and between STOCH_CPL and REF for years 1–201, respectively. Sea ice thickness shows a uniform increase throughout the entire Arctic in STOCH_UNCPL when stochastic sea ice perturbations are used. The increase in sea ice concentration occurs primarily in areas where the ice edge can be found during the melting and freezing seasons.

For the coupled stochastic simulation, a completely different picture emerges. For STOCH_CPL, sea ice thickness increase is limited to an area along the north coast of Greenland and the Canadian Arctic Archipelago area. The central and eastern Arctic, on the other hand, show reduced sea ice thicknesses. A somewhat similar pattern is found for sea ice concentration changes in STOCH_CPL. These patterns point towards a redistribution of sea ice cover and thickness from the east to the west as discussed above. Owing to the weakened ice, sea ice drift is increased. But while in the uncoupled case STOCH_UNCPL, this redistribution seems to lead to an increase in sea ice production during the freezing season, which compensates for the drift and opening of leads, some atmospheric feedback mechanism appears to counteract this increased sea ice production in STOCH_CPL. As a consequence, sea ice is redistributed without any build-up in sea ice volume.

This hypothesis is further substantiated by figure 3, which shows sea ice drift along with its changes owing to the stochastic scheme. While in STOCH_UNCPL, sea ice velocities are slightly decreased in the central Arctic (anticlockwise arrows), they are increased in STOCH_CPL (clockwise arrows). The differences between the simulations can be explained as follows: during the transient phase of the integration, STOCH_UNCPL experiences a slight increase in sea ice velocities (not shown). The increased sea ice thickness distribution is still accumulating and increased sea ice thicknesses do not yet balance the influence from the effective weakening of the sea ice strength owing to the stochastic perturbations. After this transient phase, though, sea ice drift tends to be reduced, because thicker sea ice is capable of balancing the direct impact of the P^* perturbations.

The velocity changes in STOCH_CPL are quite different. Most of the drift in the central Arctic is increased or slightly redirected towards the north coasts of Canada, the Canadian Arctic Archipelago and Greenland. Due to the fact that there is no accumulation in Arctic sea ice, the

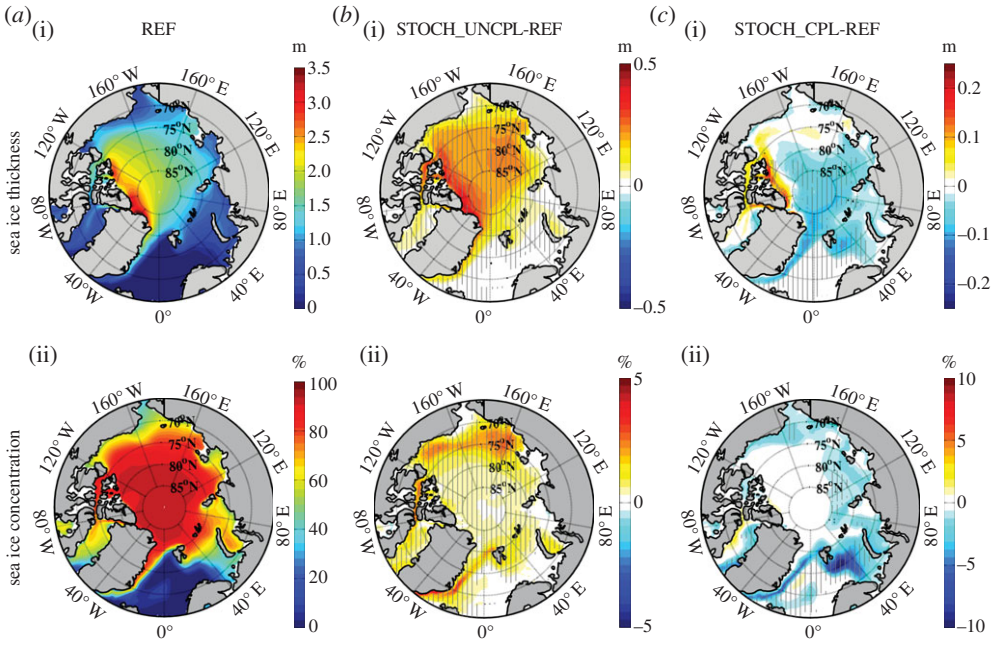

Figure 2. (*a*) Annual mean (i) sea ice thickness (m) and (ii) sea ice concentration (%) for REF, years 1–201. (*b*) Difference in annual mean (i) sea ice thickness (m) and (ii) sea ice concentration (%) between STOCH_UNCPL and REF, years 1–102. (*c*) Same as (*b*), but for the difference between STOCH_CPL and REF, years 1–201. Hatched areas indicate differences statistically significant at the 5% level, using a Wilcoxon signed-rank test for the paired samples of STOCH_UNCPL-REF and a Wilcoxon–Mann–Whitney rank-sum test for the independent samples of STOCH_CPL-REF [44]. Note the different contour intervals.

effective decrease in sea ice strength is not balanced. Therefore, the changes in the sea ice velocity field resemble more the transient phase of STOCH_UNCPL.

(iv) Annual cycle

Figure 4 illustrates the annual cycle of monthly mean sea ice volume, sea ice area and the thermodynamic growth rate for REF for the Northern as well as for the Southern Hemisphere (*a*(i–iii)); also shown are their changes when the stochastic sea ice parametrization is used (*b*(i–iii)). Sea ice volume in the Southern Hemisphere is only a fraction of that in the Arctic. This is especially true when the respective summer months are compared. For sea ice area, a similar behaviour is found with the exception that wintertime sea ice extent in the Antarctic exceeds that in the Arctic. The annual cycle of thermodynamic growth rates is very similar in the two hemispheres.

The influence of the stochastic sea ice parametrization on the annual cycle of Arctic sea ice volume in the coupled model follows that of the sea ice volume in REF (figure 4, bottom row) with the largest (smallest) absolute differences found in winter (summer). The influence of the stochastic parametrization in the uncoupled integration mostly lacks any seasonality and is much larger in magnitude. The response in STOCH_UNCPL, however, took several decades to fully develop. A comparison for the first few years of the STOCH_UNCPL integration yields much more similar results in the magnitude of changes for the coupled and uncoupled model (not shown). The seasonality of the response for sea ice area in both models is more similar than that for the volume. However, the response is shifted by about 0.3–0.4 10^6 km^2.

(v) Growth rates and atmospheric feedback

Changes in the thermodynamic growth rates in the bottom right panel of figure 4 hint at a negative atmospheric feedback mechanism in STOCH_CPL. While for STOCH_CPL melting is reduced in spring and summer and freezing is reduced in autumn and winter, the opposite changes are found

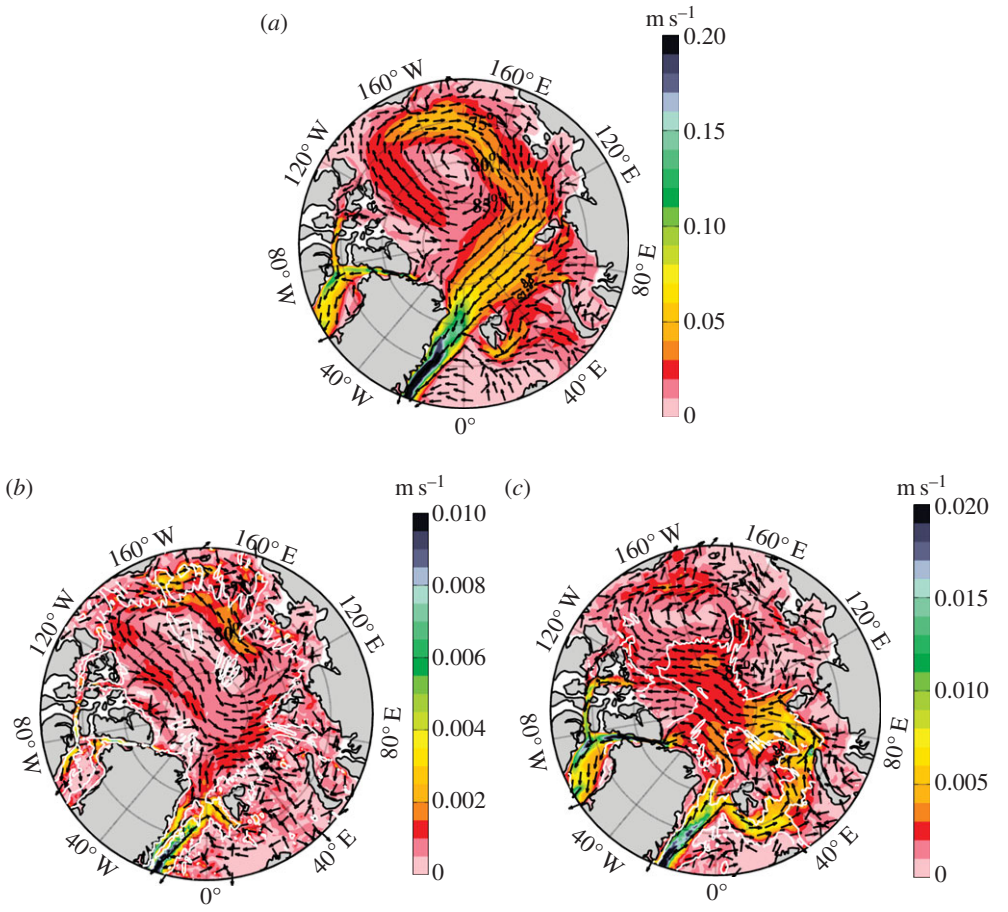

Figure 3. (*a*) Annual mean sea ice velocity (m s^{-1}) for REF, years 1–201. (*b*) Difference in annual mean sea ice velocity (m s^{-1}) between STOCH_UNCPL and REF, years 1–102. (*c*) Same as (*b*), but for the difference between STOCH_CPL and REF, years 1–201. Arrows are normalized and white contour lines enclose areas where the zonal and/or meridional velocity component is significantly different from zero at the 5% level, using the same tests as in figure 2. Note the different contour intervals.

for STOCH_UNCPL. The behaviour of the response for STOCH_UNCPL can be explained as follows: shifting of sea ice during the freezing season opens up leads and creates open water areas. As fluxes are fixed and the atmosphere is seen as an infinite source or sink of heat in the uncoupled set-up, open water can freeze over and quickly produce more ice. This newly created ice then drifts away, and the process is repeated. On the other hand, sea ice thickness and concentration is increased in the areas of convergent motion, which leads to decreased growth rates in those regions. Still, the enhanced production of sea ice in areas of open water is stronger than the reduction of growth rates owing to increased plastic deformation. As a result mean growth rates and therefore sea ice volume are increased compared with the reference simulation. In the annual mean, the increase in sea ice growth rates during freezing seasons has a larger impact than the increase in melt during spring and summer, especially during the first 20–30 years of the transient phase.

For STOCH_CPL, the response to the stochastic sea ice parametrization is different. The atmosphere is no longer an infinite source or sink of energy, because it can respond to the sea ice changes. A feedback mechanism that explains the differences in the coupled and uncoupled set-up is connected to the sea ice thickness and opening of leads during autumn and winter. At

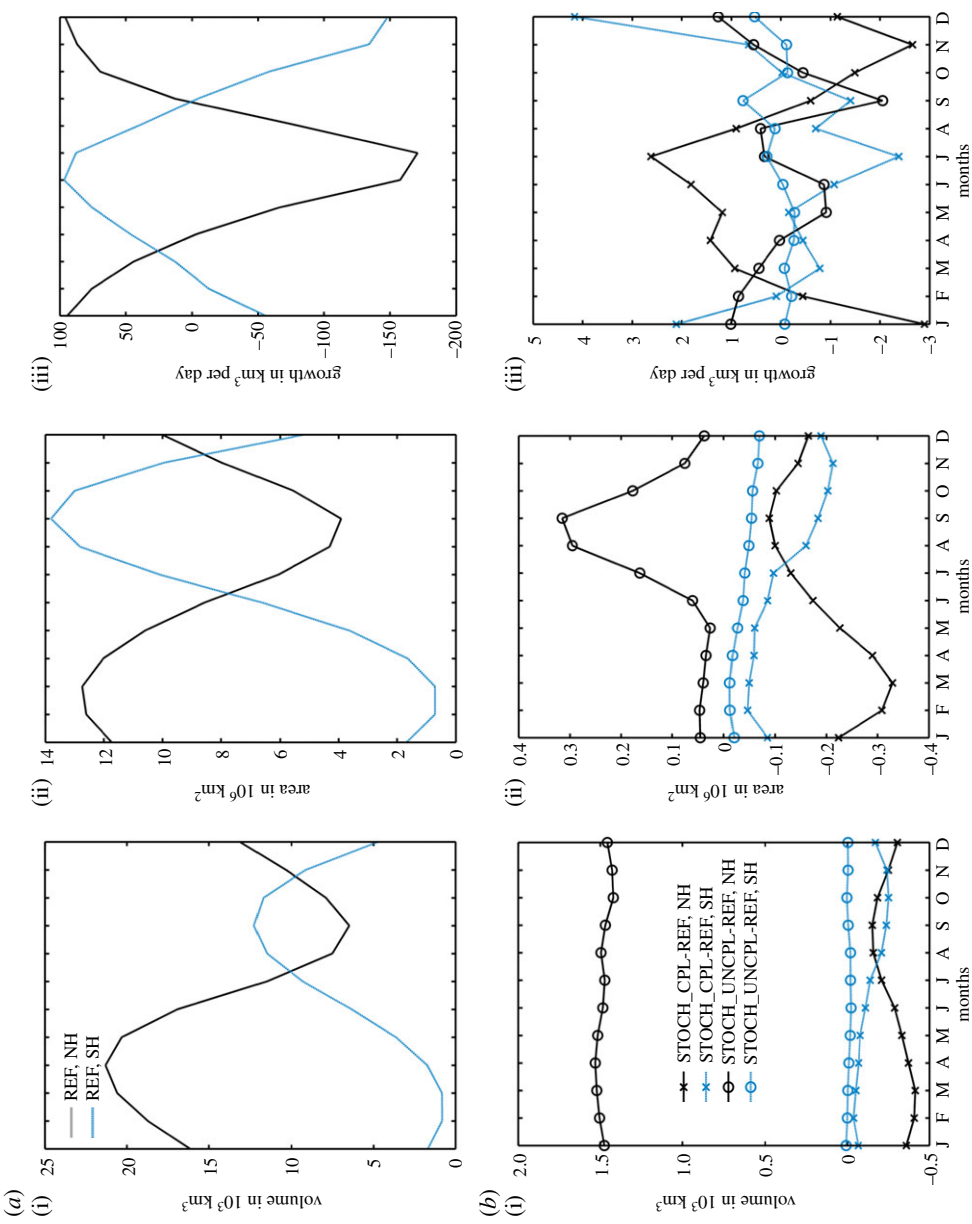

Figure 4. (*a*) Annual cycle of monthly mean (i) sea ice volume (10^3 km^3), (ii) sea ice area (10^6 km^2) and (iii) thermodynamic growth rates (km^3 day^{-1}) for REF, years 1–201. (*b*) Difference in the annual cycle of monthly mean (i) sea ice volume (10^3 km^3), (ii) sea ice area (10^6 km^2) and (iii) thermodynamic growth rates (km^3 day^{-1}) between STOCH_CPL and REF (crosses), years 1–201, as well as STOCH_UNCPL and REF (circles), years 1–102. Black is for the Northern Hemisphere and blue for the Southern Hemisphere.

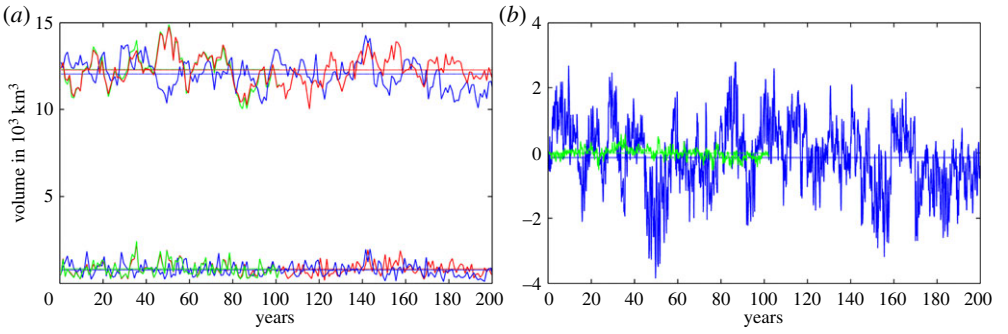

Figure 5. (*a*) Southern Hemisphere total sea ice volume (10^3 km^3) for REF (red), STOCH_CPL (blue) and STOCH_UNCPL (green); results are shown for March (lower curves) and September (upper curves). (*b*) Monthly mean difference in Southern Hemisphere sea ice volume (10^3 km^3) between STOCH_CPL and REF (blue) as well as STOCH_UNCPL and REF (green). Coloured horizontal lines show respective mean values.

the beginning of the freezing season production of sea ice is increased in the areas of open water created in the east by enhanced sea ice drift. But because the atmosphere in STOCH_CPL is now heated from the ocean, it reacts in the coupled system and becomes warmer over open water. This will reduce the heat loss of the ocean and hence freezing rates in open water; sea ice production in open water areas, consequently, is no longer sufficiently strong to compensate for the effect of reduced ice growth owing to piled up ice further to the west. Therefore, the mean growth rate is reduced in STOCH_CPL when compared with REF. Further support for the existence of such a negative feedback mechanisms comes from a slight increase in near-surface atmospheric air temperatures in January and February over the eastern Arctic, slightly increased (reduced) ocean temperatures in most of the eastern (western) Arctic and slightly reduced mixed layer depth in the central Arctic owing to reduced growth rates (not shown). In STOCH_UNCPL, these changes are very different, with generally slightly decreased ocean temperatures and increased mixed layer depth owing to an increase in growth rates and lower water temperatures (not shown).

In summary, it is argued that in the coupled model the slight decrease in sea ice growth during winter owing to the stochastic sea ice scheme is sufficient to prevent a gradual build-up of sea ice volume in the Arctic that is observed in the uncoupled model.

(b) Antarctic sea ice

(i) Volume

The difference in effects between Northern and Southern Hemisphere sea ice is especially pronounced when the impact of the stochastic sea ice parametrization is considered in the uncoupled simulation (figure 4). While the volume increase in the Arctic is able to accumulate over time this is not possible in the Antarctic owing to the almost complete loss of sea ice in austral summer. Figure 5 shows the time series of monthly mean sea ice volume for the Southern Hemisphere, for March and September and all three simulations. The Antarctic sea ice volume strongly increases from its minimum in March to its maximum in September (see also figure 4, *a*(i–iii)). Antarctic sea ice volume shows substantial interannual to decadal variability. Compared with the Arctic (figure 1), however, there is much less multi-decadal variability which again is consistent with a relative lack of memory owing to Antarctic sea ice loss in summer.

The right panel of figure 5 illustrates the differences in sea ice volume between the integration with and without the stochastic ice strength scheme for the uncoupled and coupled model. It is confirmed that in contrast to the Arctic there is no change in the mean Southern Hemisphere sea ice volume, neither for STOCH_UNCPL nor for STOCH_CPL. As sea ice area and volume are

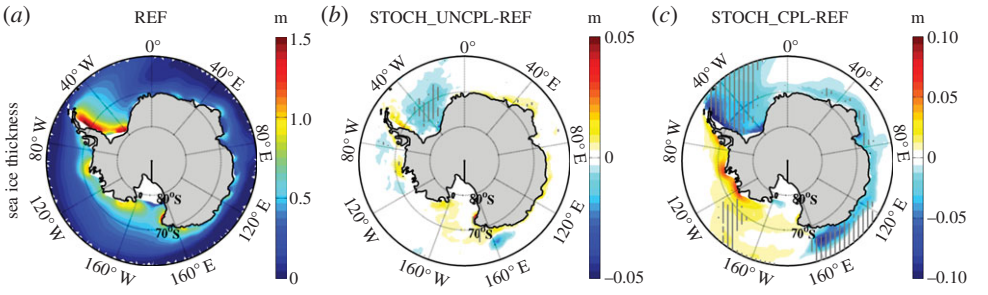

Figure 6. (*a*) Annual mean sea ice thickness (m) for REF, years 1–201. (*b*) Difference in annual mean sea ice thickness (m) between STOCH_UNCPL and REF, years 1–102. (*c*) Same as (*b*), but for the difference between STOCH_CPL and REF, years 1–201. Hatched areas indicate differences statistically significant at the 5% level, using the same tests as in figure 2. Note the different contour intervals.

strongly reduced during the summer months changes in sea ice thickness can hardly accumulate over time.

(ii) Regional impacts

The annual mean sea ice thickness distribution of REF and its changes resulting from the use of the stochastic parametrization are shown in figure 6. Sea ice is about two to three times thinner in the Southern Hemisphere than it is in the Northern Hemisphere. As a result, changes in thickness owing to the stochastic perturbations are also smaller than in the Northern Hemisphere. In addition, the distribution of landmasses is very different in the Northern Hemisphere; whereas the coastlines of the Canadian Arctic Archipelago present ideal conditions for a stochastic sea ice strength parametrization to have an impact on the mean state, such confining topographic structures are largely absent in the Southern Hemisphere high latitudes. Interestingly, the largest thickness changes in STOCH_UNCPL are located along the coast of Antarctica, where the stochastic scheme leads to increased sea ice thickness. Those are areas of convergent or shear drift where sea ice might also survive the melting season.

For STOCH_CPL, the changes are again somewhat different. Instead of sea ice piling up near the east coast of the Antarctic Peninsula, sea ice is drifted eastward. This leads to a shift of ice from the west to the east. In addition, the changes are larger in amplitude and in scale than in STOCH_UNCPL. One reason might be the stronger increase in eastward sea ice drift and the change in vertically integrated barotropic streamfunction of the ocean (not shown). The latter shows an enhanced eastward flow and enhanced gyre strength. Even though this is also observable in STOCH_UNCPL, the impact in STOCH_CPL is larger, with an annual mean increase of about 0.5–1 Sv compared with about 2 Sv for the Weddell Gyre, respectively.

(c) Remote impacts

Figure 7 shows the time series of the annual mean Atlantic meridional overturning circulation (AMOC) at about 45° N and 1 km depth for all three simulations. As has been the case for the Arctic sea ice volume and area, the AMOC is highly variable with large variations from year to year. It should also be noted that the AMOC is correlated to the Arctic sea ice volume and area, as it transports heat to the north and is driven by the North Atlantic Deep Water formation which, in turn, influences or is influenced, respectively, by sea ice cover and growth rates [46,47].

When looking at the differences between the stochastic simulations and REF in the figure 7*b* no large change in the AMOC can be observed for STOCH_UNCPL. This is probably due to the fact that changes in sea ice thickness are mostly occurring in the central Arctic and are quite small from year to year. The increase in AMOC in STOCH_CPL is presumably just a result of sampling

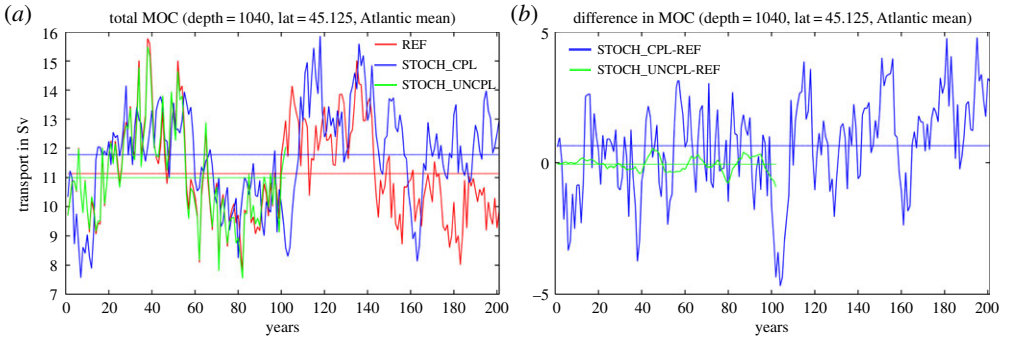

Figure 7. (*a*) Time series of the annual mean AMOC (Sv) at 45°N and a depth of approx. 1000 m for REF (red), STOCH_CPL (blue) and STOCH_UNCPL (green). (*b*) Corresponding time series of the difference in AMOC (Sv) between STOCH_CPL and REF (blue) as well as STOCH_UNCPL and REF (green). Coloured horizontal lines show respective mean values.

variability caused by the multidecadal variability of the AMOC. Similar results were found for other oceanic and atmospheric parameters in non-polar regions of the globe (not shown). In summary, it turns out that significant changes in the mean climate caused by the stochastic perturbations are very much confined to high latitudes.

4. Conclusion

A symmetric stochastic perturbation of the sea ice strength parameter based on Juricke *et al.* [30] has been implemented in the coupled climate model ECHAM6-FESOM. A set of coupled and uncoupled multi-decadal experiments has been carried out in order to explore the impact that the stochastic sea ice parametrization has on the mean climate in coupled compared with uncoupled models.

In the Arctic, including a stochastic sea ice parametrization in an uncoupled sea ice–ocean model results in an increase in sea ice thickness and volume by some 10–20% (depending on the season). This increase can be explained by the fact that the stochastic perturbations of the sea ice strength lead to an effective weakening of the sea ice, because small stochastic values of the ice strength are more influential than large ones. As a result, convergent sea ice drift is enhanced, which leads to an accumulation of sea ice thickness in the central Arctic and especially along the coastlines in the western Arctic. The first 20–30 years of uncoupled integration with the stochastic scheme can be seen as a transient phase. During this phase, sea ice thickness increase accumulates and increased sea ice production in areas of newly opened water leads to an increase in sea ice volume. After the transient phase, the sea ice–ocean system reaches a new quasi-equilibrium state in which the increased sea ice thickness counteracts the effective weakening of the sea ice caused by the ice strength perturbations. Sea ice volume is no longer increased. In contrast to the Arctic, the influence of the stochastic sea ice parametrization on the mean climate of the Antarctic is relatively small in the uncoupled model. This can be explained by the fact that Antarctic sea ice almost completely vanishes during austral summer which inhibits the small temporal accumulation of stochastic effects.

The impact of the stochastic sea ice parametrization on the mean climate of the coupled model ECHAM6-FESOM turns out to be very different. The mean sea ice volume in the Arctic and Antarctic remains largely unchanged with the stochastic scheme switched on. In the Arctic, this can be explained by the fact that in an integrated sense the increase of sea ice thickness north of Greenland and the Canadian Arctic Archipelago is accompanied by a loss of sea ice in the central and eastern Arctic. This reflects the increased transport of sea ice from the eastern to the western Arctic which is also reflected in increased sea ice velocities. The same argument holds for the

Antarctic. However, in the Southern Hemisphere, sea ice shows evidence of being increasingly transported eastward and changes in thicknesses are smaller than in the north.

The fact that the coupled system responds differently to a stochastic sea ice parametrization compared with an uncoupled model highlights the fact that care has to be taken when results from uncoupled experiments are extrapolated to the coupled climate system. The results suggest that by incorporating the atmosphere a negative feedback is introduced that prevents the stochastic effect in the coupled model from accumulating. Given the slowness of the accumulation process in the uncoupled model (figure 1), it is likely that even a relatively weak negative atmospheric feedback would be sufficient to prevent the stochastic sea ice parametrization from influencing the mean climate of the coupled system. Given the strong variability of sea ice on a wide range of timescales, therefore, pinning down the exact negative mechanisms is challenging.

However, one reason for the discrepancies between the coupled and the uncoupled simulation might have to do with the atmospheric response (or lack thereof) to an increased amount of open water during the freezing season owing to the stochastic sea ice parametrization. In the uncoupled stochastic simulation, the fluxes are fixed, and therefore the atmosphere is prevented from adjusting and hence reducing the amount of sea ice production in open water areas. This unrealistically large productivity outweighs the effect of reduced sea ice growth in the western Arctic owing to increased sea ice thickness. In the coupled model, the incorporation of the stochastic scheme also leads to increased sea ice production in open waters; the magnitude of this ice growth, however, is much reduced owing to the adjustment of the overlying atmosphere. The adjustment of the atmosphere helps to reduce the sea ice production increase and, hence, the reduction of growth rates in the western Arctic owing to thicker sea ice becomes comparable or even larger than the increase in growth rates owing to the generation of open water through the stochastic sea ice parametrization.

The remote response of the climate system in non-polar regions to the incorporation of the stochastic sea ice strength scheme turns out to be rather weak. This may be a result of the fact that the mean response in the polar regions to the stochastic sea ice parametrization is relatively low and that the level of natural variability is high. However, it is also possible that the mean influence on the Atlantic overturning circulation is relatively weak, because the coupled model ECHAM6-FESOM is relatively insensitive to buoyancy anomalies in the Labrador Sea region [42]. Given that Labrador Sea convection is believed to be strongly affected by freshwater anomalies of Arctic origin [48] a stronger response of the overturning might be found in other more sensitive models.

While the impact of the stochastic sea ice strength parametrization on the mean climate of the coupled model seems to be somewhat reduced when compared to the impact in the uncoupled model, it should be pointed out that tests in an ensemble prediction framework suggest that the stochastic sea ice parametrization does lead to additional spread during the early part of the integration [49]. Hence, the stochastic parametrization described here might become useful when it comes to coupled data assimilation and uncertainty estimation in monthly and seasonal polar prediction. Another promising direction of future research will be to look at stochastic formulations of other sea ice aspects. Given the climate relevance of the sea ice-albedo feedback the development of a stochastic sea ice albedo scheme appears to be a promising way forward. In addition, the P^* perturbations presented here might again show quite different effects on the mean climate when combined with other stochastic parametrizations of the sea ice model and/or using a different configuration of the parametrization, for example yet another more sophisticated spatial correlation scheme.

Acknowledgements. We are indebted to our colleagues Dr Helge Goessling, Thomas Rackow and Dr Dmitry Sidorenko for various fruitful discussions during the course of this study. We also thank the two reviewers for their helpful and much appreciated remarks and comments.

Funding statement. This study benefited from support of the REKLIM and TORUS-MiKlip projects. Computational resources were made available by the German Climate Computing Center (DKRZ) through support from the German Federal Ministry of Education and Research (BMBF), project ba0771, and by the North-German Supercomputing Alliance (HLRN), project hbk00032.

References

1. Hendricks S, Gerland S, Smedsrud LH, Haas C, Pfaffhuber AA, Nilsen F. 2011 Sea-ice thickness variability in Storfjorden, Svalbard. *Ann. Glaciol.* **52**, 61–68. (doi:10.3189/172756411795931561)
2. Laxon S, Peacock N, Smith D. 2003 High interannual variability of sea ice thickness in the Arctic region. *Nature* **425**, 947–950. (doi:10.1038/nature02050)
3. Kwok R, Rothrock DA. 2009 Decline in Arctic sea ice thickness from submarine and ICESat records: 1958–2008. *Geophys. Res. Lett.* **36**, L15501. (doi:10.1029/2009GL039035)
4. Kwok R, Cunningham GF, Wensnahan M, Rigor I, Zwally HJ, Yi D. 2009 Thinning and volume loss of the Arctic Ocean sea ice cover: 2003–2008. *J. Geophys. Res.* **114**, C07005. (doi:10.1029/2009JC005312)
5. Turner J, Bracegirdle TJ, Phillips T, Marshall GJ, Hosking JS. 2013 An initial assessment of Antarctic sea ice extent in the CMIP5 models. *J. Clim.* **26**, 1473–1484. (doi:10.1175/JCLI-D-12-00068.1)
6. Johnson M *et al.* 2012 Evaluation of Arctic sea ice thickness simulated by Arctic Ocean model intercomparison project models. *J. Geophys. Res.* **117**, C00D13. (doi:10.1029/2011JC007257)
7. Stroeve JC, Kattsov V, Barrett A, Serreze M, Pavlova T, Holland M, Meier WN. 2012 Trends in Arctic sea ice extent from CMIP5, CMIP3 and observations. *Geophys. Res. Lett.* **39**, L16502. (doi:10.1029/2012GL052676)
8. Holland MM, Bailey DA, Vavrus S. 2011 Inherent sea ice predictability in the rapidly changing Arctic environment of the community climate system model, version 3. *Clim. Dyn.* **36**, 1239–1253. (doi:10.1007/s00382-010-0792-4)
9. Chevallier M, Salas-Mélia D. 2012 The role of sea ice thickness distribution in the arctic sea ice potential predictability: a diagnostic approach with a coupled GCM. *J. Clim.* **25**, 3025–3038. (doi:10.1175/JCLI-D-11-00209.1)
10. Fichefet T, Maqueda MAM. 1997 Sensitivity of a global sea ice model to the treatment of ice thermodynamics and dynamics. *J. Geophys. Res.* **102**, 12 609–12 646. (doi:10.1029/97JC00480)
11. Hibler WD. 1979 A dynamic thermodynamic sea ice model. *J. Phys. Oceanogr.* **9**, 815–846. (doi:10.1175/1520-0485(1979)009<0815:ADTSIM>2.0.CO;2)
12. Hunke EC, Lipscomb WH. 2010 CICE: The Los Alamos sea ice model, documentation and software user's manual, version 4.1. Tech. Rep. LA-CC-06-012, T-3 Fluid Dynamics Group, Los Alamos National Laboratory, Los Alamos, USA, 76 pp.
13. Girard L, Bouillon S, Weiss J, Amitrano D, Fichefet T, Legat V. 2011 A new modeling framework for sea-ice mechanics based on elasto-brittle rheology. *Ann. Glaciol.* **52**, 123–132. (doi:10.3189/172756411795931499)
14. Lemieux JF, Knoll D, Tremblay B, Holland DM, Losch M. 2012 A comparison of the Jacobian-free Newton–Krylov method and the EVP model for solving the sea ice momentum equation with a viscous-plastic formulation: a serial algorithm study. *J. Comput. Phys.* **231**, 5926–5944. (doi:10.1016/j.jcp.2012.05.024)
15. Losch M, Fuchs A, Lemieux JF, Vanselow A. 2013 A parallel Jacobian-free Newton–Krylov solver for a coupled sea ice-ocean model. *J. Comput. Phys.* **257**, 901–911. (doi:10.1016/j.jcp.2013.09.026)
16. Lorenz EN. 1996 Predictability: a problem partly solved. *Proc. Semin. Predictability*, Reading, United Kingdom, ECMWF, **1**, 1–19.
17. Wilks DS. 2005 Effects of stochastic parametrizations in the Lorenz '96 system. *Q. J. R. Meteorol. Soc.* **131**, 389–407. (doi:10.1256/qj.04.03)
18. Arnold HM, Moroz IM, Palmer TN. 2013 Stochastic parametrizations and model uncertainty in the Lorenz '96 system. *Phil. Trans. R. Soc. A* **371**, 20110479. (doi:10.1098/rsta.2011.0479)
19. Buizza R, Miller M, Palmer TN. 1999 Stochastic representation of model uncertainties in the ECMWF ensemble prediction system. *Q. J. R. Meteorol. Soc.* **125**, 2887–2908. (doi:10.1002/qj.49712556006)
20. Weisheimer A, Palmer TN, Doblas-Reyes FJ. 2011 Assessment of representations of model uncertainty in monthly and seasonal forecast ensembles. *Geophys. Res. Lett.* **38**, L16703. (doi:10.1029/2011GL048123)
21. Shutts G. 2005 A kinetic energy backscatter algorithm for use in ensemble prediction systems. *Q. J. R. Meteorol. Soc.* **131**, 3079–3102. (doi:10.1256/qj.04.106)

22. Jung T, Palmer TN, Shutts GJ. 2005 Influence of a stochastic parameterization on the frequency of occurrence of North Pacific weather regimes in the ECMWF model. *Geophys. Res. Lett.* **32**, L23811. (doi:10.1029/2005GL024248)
23. Berner J, Shutts GJ, Leutbecher M, Palmer TN. 2009 A spectral stochastic kinetic energy backscatter scheme and its impact on flow-dependent predictability in the ECMWF ensemble prediction system. *J. Atmos. Sci.* **66**, 603–626. (doi:10.1175/2008JAS2677.1)
24. Lott F, Guez L, Maury P. 2012 A stochastic parameterization of non-orographic gravity waves: formalism and impact on the equatorial stratosphere. *Geophys. Res. Lett.* **39**, L06807. (doi:10.1029/2012GL051001)
25. Lin JW-B, Neelin JD. 2002 Considerations for stochastic convective parameterization. *J. Atmos. Sci.* **59**, 959–975. (doi:10.1175/1520-0469(2002)059<0959:CFSCP>2.0.CO;2)
26. Plant RS, Craig GC. 2008 A stochastic parameterization for deep convection based on equilibrium statistics. *J. Atmos. Sci.* **65**, 87–105. (doi:10.1175/2007JAS2263.1)
27. Lin JW-B, Neelin JD. 2000 Influence of a stochastic moist convective parameterization on tropical climate variability. *Geophys. Res. Lett.* **27**, 3691–3694. (doi:10.1029/2000GL011964)
28. Bright DR, Mullen SL. 2002 Short-range ensemble forecasts of precipitation during the southwest monsoon. *Weather Forecast.* **17**, 1080–1100. (doi:10.1175/1520-0434(2002)017<1080:SREFOP>2.0.CO;2)
29. Li X, Charron M, Spacek L, Guillem C. 2008 A regional ensemble prediction system based on moist targeted singular vectors and stochastic parameter perturbations. *Mon. Weather Rev.* **136**, 443–462. (doi:10.1175/2007MWR2109.1)
30. Juricke S, Lemke P, Timmermann R, Rackow T. 2013 Effects of stochastic ice strength perturbation on arctic finite element sea ice modeling. *J. Clim.* **26**, 3785–3802. (doi:10.1175/JCLI-D-12-00388.1)
31. Brankart J-M. 2013 Impact of uncertainties in the horizontal density gradient upon low resolution global ocean modelling. *Ocean Model.* **66**, 64–76. (doi:10.1016/j.ocemod.2013.02.004)
32. Williams PD. 2012 Climatic impacts of stochastic fluctuations in air-sea fluxes. *Geophys. Res. Lett.* **39**, L10705. (doi:10.1029/2012GL051813)
33. Palmer TN. 2012 Towards the probabilistic Earth-system simulator: a vision for the future of climate and weather prediction. *Q. J. R. Meteorol. Soc.* **138**, 841–861. (doi:10.1002/qj.1923)
34. Sidorenko D *et al.* 2014 Towards multi-resolution global climate modeling with ECHAM6-FESOM. Part I: model formulation and mean climate. *Clim. Dyn.*
35. Stevens B *et al.* 2013 Atmospheric component of the MPI-M earth system model: ECHAM6. *J. Adv. Model. Earth Syst.* **5**, 146–172. (doi:10.1002/jame.20015)
36. Valcke S. 2013 The OASIS3 coupler: a European climate modelling community software. *Geosci. Model Dev.* **6**, 373–388. (doi:10.5194/gmdd-5-2139-2012)
37. Danilov S, Kivman G, Schröter J. 2004 A finite-element ocean model: principles and evaluation. *Ocean Model.* **6**, 125–150. (doi:10.1016/S1463-5003(02)00063-X)
38. Wang Q, Danilov S, Schröter J. 2008 Finite element ocean circulation model based on triangular prismatic elements, with application in studying the effect of topography representation. *J. Geophys. Res.* **113**, C05015. (doi:10.1029/2007JC004482)
39. Timmermann R, Danilov S, Schröter J, Böning C, Sidorenko D, Rollenhagen K. 2009 Ocean circulation and sea ice distribution in a finite element global sea ice-ocean model. *Ocean Model.* **27**, 114–129. (doi:10.1016/j.ocemod.2008.10.009)
40. Sidorenko D, Wang Q, Danilov S, Schröter J. 2011 FESOM under coordinated ocean-ice reference experiment forcing. *Ocean Dyn.* **61**, 881–890. (doi:10.1007/s10236-011-0406-7)
41. Wang Q, Danilov S, Sidorenko D, Timmermann R, Wekerle C, Wang X, Jung T, Schröter J. 2013 The finite element sea ice–ocean model (FESOM): formulation of an unstructured-mesh ocean general circulation model. *Geosci. Model. Dev. Discuss.* **6**, 3893–3976. (doi:10.5194/gmdd-6-3893-2013)
42. Rackow *et al.* 2014 In preparation. Towards multi-resolution global climate modeling with ECHAM6-FESOM. Part II: Climate variability.
43. Harder M. 1996 Dynamics, roughness, and age of Arctic sea ice: numerical investigations with a large-scale model. Reports on Polar Research, Alfred Wegener Institute for Polar- and Marine Research, Bremerhaven, Germany, **203**, 127 p.
44. Wilks DS. 2011 *Statistical methods in the atmospheric sciences*, 3rd edn. International Geophysics Series. Waltham, MA: Academic Press.

45. Large WG, Yeager SG. 2009 The global climatology of an interannually varying air-sea flux data set. *Clim. Dyn.* **33**, 341–364. (doi:10.1007/s00382-008-0441-3)
46. Mahajan S, Zhang R, Delworth TL. 2011 Impact of the Atlantic meridional overturning circulation (AMOC) on Arctic surface air temperature and sea ice variability. *J. Clim.* **24**, 6573–6581. (doi:10.1175/2011JCL14002.1)
47. Jahn A, Holland MM. 2013 Implications of Arctic sea ice changes for North Atlantic deep convection and the meridional overturning circulation in CCSM4-CMIP5 simulations. *Geophys. Res. Lett.* **40**, 1206–1211. (doi:10.1002/grl.50183)
48. Dickson RR, Meincke J, Malmberg S-A, Lee AJ. 1988 The 'great salinity anomaly' in the Northern North Atlantic 1968–1982. *Prog. Oceanogr.* **20**, 103–151. (doi:10.1016/0079-6611(88)90049-3)
49. Juricke, J, Goessling HF, Jung T. 2014 Potential sea ice predictability and the role of stochastic sea ice perturbations. *Geophys. Res. Lett*.